Tunable Non-Hermitian Acoustic Filter

S. Puri,[1,†] J. Ferdous,[1,†] A. Shakeri,[1] A. Basiri,[2] M. Dubois,[3] and H. Ramezani [1,*]

[1]*Department of Physics and Astronomy, University of Texas Rio Grande Valley, Edinburg, Texas 78539, USA*
[2]*School of ECEE, Arizona State University, Tempe, Arizona 85287, USA*
[3]*Multiwave Imaging SAS, Marseille 13013, France*

We propose, design, and experimentally test a non-Hermitian acoustic superlattice that acts as a tunable precise filter. The superlattice is composed of two concatenated sublattices. The first sublattice is Hermitian, while the other can be adjusted to be Hermitian or non-Hermitian. The existence of non-Hermiticity, in terms of an induced loss in the second sublattice, results in the generation of absorption resonances that appear in the reflected spectrum. This provides us with a powerful knob to absorb or reflect several frequencies at will with high accuracy. The number of filtered frequencies can be controlled by designing the resonances in the first sublattice. Our proposed tunable acoustic filter can be extended to higher-frequency ranges, such as ultrasound, and other areas, such as photonics.

I. INTRODUCTION

The existence of complete band gaps makes phononic crystals attractive for many potential applications, such as vibration isolation, noise suppression, acoustic barriers, filters, waveguides, and transducers, to name a few [1–4]. However, practical frequency and band-gap tunability of phononic crystals is a major stumbling block to application in real-world devices in different technological domains [5,6]. To achieve tunability, several ideas, including thermal tuning [7], application of an external magnetic field [8–11], piezoelectric shunting [12], electromechanical tuning [13], embedded electromagnets [14], static loading [15], nonlinear effects [16–18], and acoustic trapping [19], have been proposed. The main parameters affecting the frequency and width of the band gaps, namely, lattice geometry, density, and sound-velocity contrast of the component materials constituting the phononic lattice, have been the focus of these works.

More recently, another viewpoint has emerged that embraces non-Hermiticity to propose interesting physics and control sound propagation in acoustic media [20,21]. The degree of non-Hermiticity is induced by means of an effective complex mass density and bulk modulus synthesized via loss and gain mechanisms embedded in the phononic structure. The effect of losses on acoustic wave propagation has been studied in numerous works [22–27]. However, their ubiquitous presence is neglected or minimized due to the conventionally accepted adverse effects

that they have on the performance of an acoustic material under study [28]. Recent fascinating and peculiar achievements obtained in non-Hermitian systems and specifically parity-time symmetric systems with intentionally and judiciously introduced balanced amplification and absorption mechanisms (see [29] and references within), inspire us to incorporate the degree of non-Hermiticity in acoustic systems. To date, several noticeable theoretical and experimental parity-time symmetric acoustic structures have been proposed [30–37]. Moreover, non-Hermiticity, specifically in terms of losses [38,39], is used to achieve, for instance, an extreme asymmetric acoustic response [40], experimental demonstration of acoustic asymmetric diffraction grating [41], unidirectional wave-vector manipulation in two-dimensional space [42], experimental realization of a higher-order topology in an acoustic crystal [43], a topologically protected exceptional point [44], asymmetric loss-induced perfect sound absorption [45], perfect absorption through a subwavelength medium [46], loss-induced angle-dependent absorption [47], anomalous energy transport with exceptional points [48], stabilization of acoustic modes using Helmholtz and quarter-wave resonators tuned to exceptional points, [49], conditional simultaneous unidirectional zero reflection, and extraordinarily high transmission [50].

Here, we theoretically propose and experimentally demonstrate another application of non-Hermiticity (losses in a phononic lattice): a tunable acoustic filter. Our proposed phononic lattice is composed of two sublattices: one is a Hermitian sublattice, which we refer to as the first sublattice, and another one with tunable non-Hermiticity, which we refer to it as the second sublattice. This

---

construction results in a tunable filter that works based on reflection, in which undesired frequencies are absorbed by the losses and the desired signal is reflected back. Altering the degree of non-Hermiticity provides an effective tuning parameter to absorb the frequencies that are going to be eliminated. Notably, here the contrast between the resonances of the two sublattices results in rich dynamics.

II. MODEL

The schematic of the lattice that we use in our simulations is depicted in Fig. 1. We assume that the lattice contains 20 hollow cuboids, which are concatenated to each other in the direction of propagation of the acoustic pressure field, x. Furthermore, they are either square cuboid, five with $7 \times 7 \times 7$ cm^3 volume in the first sublattice and five with $9.3 \times 9.3 \times 9.3$ cm^3 volume in the second sublattice, or rectangular cuboid with $7 \times 2.3 \times 2.3$ cm^3 volume that connects the square cuboids. In our simulations, we consider that all cuboids are made from polylactic acid (PLA), are hollow, and are filled with air. The density of air throughout the volume is $\rho = 1.4$ kg/m^3. Furthermore, we assume that the bulk modulus in the rectangular cuboids of both first and second sublattices and the square cuboids of the first sublattice is given by $\epsilon = 1.01 \times 10^5$ Pa, while the effective bulk modulus of the square cuboids in the second sublattice is given by $\epsilon = 1.01 \times 10^5 (1 + ia)$ Pa. The complex bulk modulus effectively describes the intrinsic or induced material loss, and a represents the effective loss parameter. In practice, a is a function of frequency,

so we start our study by assuming that a remains constant within a range of frequencies that we consider. We will show in Sec. III that an induced loss in our model can be created using side holes, the magnitude of which can be controlled by adjusting the hole dimensions, which effectively describes the value of parameter a. In this way, we capture the frequency dependence of a as well. The experimental results will show that our choice of effective model has an acceptable accuracy.

In our simulations, all boundary conditions, except input and output ports, are a sound hard boundary or a wall, which means that in a constant fluid density ρ_c the normal derivative of pressure is zero at the boundary, $\partial p_t / \partial \mathbf{n} = 0$. The input and output ports [see Fig. 1(a)] are radiation boundary conditions for a plane wave.

The unit cell of each sublattice is made of two types of cuboids: square and rectangular cuboids. Thus, the first five unit cells create a periodic passive or Hermitian sublattice, while for $a \neq 0$ the second five unit cells make a non-Hermitian sublattice. The non-Hermitian sublattice here does not have any gain component and is only composed of passive and loss components. While there are no natural acoustic gain materials, in recent years, there have been a few proposals to achieve acoustic gain using feedback systems and electronic circuits [21,32,33], which, in general, are not convenient for most applications. Thus, we use a passive-loss structure and reflection in our designed tunable filter to avoid such problems.

Each of the sublattices in our system have a band structure with passbands and gaps. Due to the geometrical differences in the two sublattices, generally, the band gaps of the sublattices, irrespective of the value of a, are not identical. However, in the gaps of both sublattices, field propagation is prohibited and the incident field is reflected with zero transmission. In the passbands, the transmission amplitude of the passive lattice is not zero. However, in the passbands of the second sublattice and for nonzero values of a, the transmission might be attenuated due to dissipation. The level of dissipation depends on the value of a.

It is shown that the value of non-Hermiticity alters the width of the band gaps [51,52]. Specifically, at the so-called exceptional point, the gap between two bands becomes zero. Thus, theoretically, one could claim that field propagation in our structure could be engineered only by tuning loss in the second sublattice. This would be a consequence of changes in the gap width resulting from non-Hermiticity. Unfortunately, altering the band structure using non-Hermiticity requires a huge loss that, in practice, is not feasible. Our experimental data show that the largest value of loss we can achieve is in the order of $a \approx 0.2$. As shown in Figs. 1(c) and 1(d), such a small amount of a has a tiny effect on the band structure of the second sublattice, and this cannot be considered as an important factor in engineering the band structure of the phononic lattice.
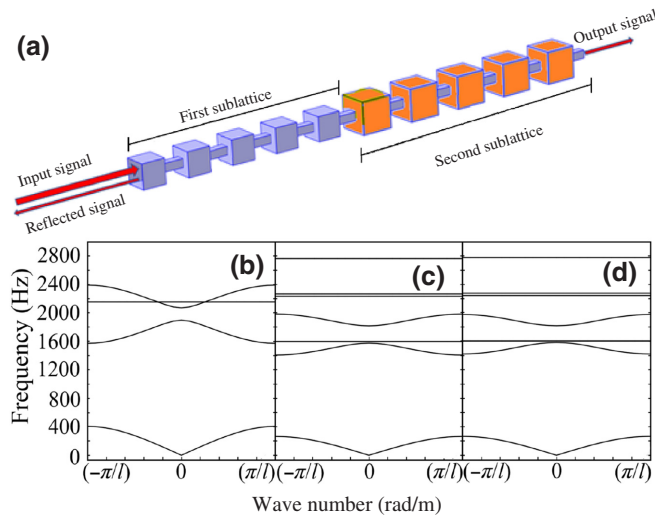

FIG. 1. (a) Schematic of the superlattice made of two sublattices and operating as a tunable acoustic filter. (b) Band structure of the first sublattice. (c) Band structure of the second sublattice with $a = 0$ and (d) band structure of the second sublattice with $a = 0.2$. Superlattice is composed of two sublattices. We observe that the difference between the band structures in (c),(d) is not considerable.

Consequently, one might naively claim that the addition of loss will not affect the dynamics in the system and the only observation might be the addition of trivial absorption in the reflected or transmitted signal. Here, we show that, surprisingly, this picture is not true and the addition of loss can result in the generation of additional "absorption" resonances. While we use the generated resonances to develop a tunable filter, one might potentially use these resonances to design tunable modulators based on non-Hermiticity.

III. THEORETICAL ANALYSIS

To show how our proposed filter works, let us first discuss the band structure of each sublattice [53]. We plot in Fig. 1(b) the band structure of an infinitely long lattice with a unit cell similar to the first sublattice in Fig. 1(a). In contrast, Figs. 1(c) and 1(d) show the band structures of an infinitely long lattice with the same unit cell as that in the second sublattice in Fig. 1(a) and with $a = 0$ and $a = 0.2$, respectively. A comparison between Figs. 1(b) and 1(c) shows that, over the frequency range 0–265 Hz, there is an overlap between the first passband of the two lattices. Thus, we expect that, if the frequency of the incident field lies in this range of frequency, it will pass through both sublattices without any absorption, as a is zero in the second sublattice. By introducing the nonzero imaginary bulk modulus, as depicted in Fig. 1(d), the first passband does not show any significant changes, and thus, the acoustic pressure can still pass through two sublattices with attenuation in the second sublattice. We plot the reflection of our lattice in Fig. 2 for $a = 0$ (blue curve) and for $a = 0.2$ (red curve) using the full-wave simulation, where the reflection amplitude is $R = W_R/W_{\text{in}}$, with

$$W_{\text{in}} = \int_S \frac{|P_0|^2}{2\rho c}, \quad W_R = \int_S \frac{|P_0 - P|^2}{2\rho c}. \quad (1)$$

In Eq. (1), P_0, P, ρ, and $c = \sqrt{\rho/\epsilon}$ are the amplitude of the incoming pressure wave, the total pressure wave, density, and speed of sound, respectively. S is the surface containing the pressure flux at the input port in Fig. 1(a).

We observe, over the frequency range 0–265 Hz, that the reflection peaks are smaller when $a \neq 0$. Obviously, as depicted in Fig. 2, at frequency ranges that the two sublattices have band gaps or the first sublattice has a band gap, we expect complete reflection, irrespective of the value of a. This matches our simulation in Fig. 2(b).

Now let us focus on the frequency ranges where the first sublattice has a passband but the second sublattice has a band gap. For instance, over the frequency range 265–410 Hz, the first sublattice has a passband and the second one has a gap, irrespective of the value of a. Thus, we expect that, due to the gap of the second sublattice, we have a total reflection. In Fig. 2 and for $a = 0$, the blue curve shows that our intuition is correct and we have a total reflection.
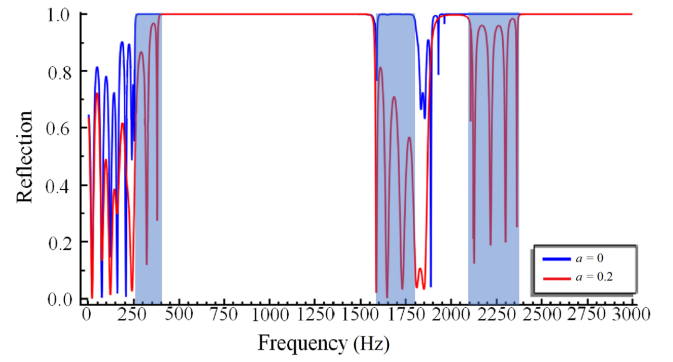

FIG. 2. Reflection of superlattice in Fig. 1 for $a = 0$ (blue curve) and $a = 0.2$ (red curve). For several frequencies in different frequency windows, we observe a large contrast in the reflection when we increase the value of a.

However, for $a \neq 0$, see the red curve, there are two resonances and, consequently, we do not have a full reflection. The same scenario occurs at other frequencies where the gap of the second sublattice overlaps with the passband of the first sublattice. The existence of such resonances is the main ingredient of our proposed filter. By introducing non-Hermiticity, we can remove specific frequencies from the reflected field. The benefit of our proposed system is in the existence of such sharp resonances, which allow for a very precise filtering process.

To understand the source of the resonances that are appearing in the reflection curve due to non-Hermiticity, let us look at the scattering matrix associated with our system. The transfer matrices of the first sublattice, M_1, and second sublattice, M_2, as a function of the reflection and transmission coefficient of each sublattice are given by

$$M_1 = \begin{pmatrix} t_1 - \frac{r_1^2}{t_1} & \frac{r_1}{t_1} \\ -\frac{r_1}{t_1} & \frac{1}{t_1} \end{pmatrix}, \quad M_2 = \begin{pmatrix} t_2 - \frac{r_2^l r_2^r}{t_2} & \frac{r_2^r}{t_2} \\ -\frac{r_2^l}{t_2} & \frac{1}{t_2} \end{pmatrix}, \quad (2)$$

where t_1 and r_1 are the transmission and reflection coefficients, respectively, of the first sublattice, and t_2, r_2^l, and r_2^r are the transmission, left reflection, and right reflection coefficients, respectively, of the second sublattice. Notably, for the second sublattice, r_2^l might not be equal to r_2^r when $a \neq 0$. We can multiply these two matrices and find the total transfer matrix, $M = M_2 M_1 = \begin{pmatrix} m_{11} & m_{12} \\ m_{21} & m_{22} \end{pmatrix}$, of our structure. Specifically, the M matrix is given by

$$M = \begin{bmatrix} \frac{(r_1^2 - t_1^2)(r_2^r r_2^l - t_2^2) - r_1 r_2^r}{t_1 t_2} & \frac{r_2^r(1 - r_1 r_2^l) + r_1 t_2^2}{t_1 t_2} \\ -\frac{t_1^2 r_2^l - r_1^2 r_2^l + r_1}{t_1 t_2} & \frac{1 - r_1 r_2^l}{t_1 t_2} \end{bmatrix}. \quad (3)$$

The transmission (t) and left and right reflection (r^l, r^r) coefficients of our one-dimensional lattice are related to

the elements of the transfer matrix:

$$t = \frac{1}{m_{22}}, \quad r^l = -\frac{m_{21}}{m_{22}}, \quad r^r = \frac{m_{12}}{m_{22}}, \quad (4)$$

and thus, the left reflection in our system will be given by

$$r^l = \frac{r_2^l(t_1^2 - r_1^2) + r_1}{1 - r_1 r_2^l}. \quad (5)$$

We can use Eq. (5) to explain the total reflection on the left side of our structure for different scenarios of band structures in the two sublattices. For example, if the incident field is at the frequency that the first lattice has a gap, then $r_1 = 1, t_1 = 0$ and, consequently, $r^l = [(-r_2^l + 1)/(1 - r_2^l)] = 1$, which means that regardless of whether the frequency of the incident field is in the band or gap of the second sublattice, we get total reflection. Now, let us consider a case in which the incident-field frequency is in the passband (gap) of the first (second) sublattice. To simplify the analysis, let us assume that the frequency of the incident beam is at the resonance of the first sublattice, and thus, $r_1 = 0, t_1 = 1$. In this case, Eq. (5) simplifies to $r^l = r_2^l$. This means that, when $a = 0$, we get a total reflection; however, when $a \neq 0$, r_2^l would be less than one due to absorption. For strong absorption, we can completely remove the reflection at certain resonance frequencies of the first sublattice. Here, it becomes clear why having the first sublattice is useful: it generates resonances, and thus, allows us to have accurate filtering of certain frequencies. Furthermore, by engineering the geometry of the first sublattice, we can design the number of resonances and their positions.

As mentioned before, for the purpose of simulations, we assume an effective and constant imaginary part of the bulk modulus, a, of air in the system in the second sublattice, which does not depend on frequency. However, in more realistic situations, the parameter a is frequency dependent. To include the effect of frequency-dependent losses and have a more realistic simulation in our tunable filter, we introduce square holes with a side length of 4.6 cm on each facet of the last five square cuboids, see Fig. 3(a). We performed the same simulation as before while this time we assume that the air in all larger cuboids have real bulk modulus ($\epsilon = 1.01 \times 10^5$ Pa). Figure 3(b) compares reflections associated with the structure with the holes (red curve) and effective bulk modulus model when $a = 0.2$. We observe that the effective model nicely matches the more realistic model.

IV. EXPERIMENTAL DEMONSTRATION

To demonstrate experimentally the proposed design of the tunable acoustic filter, we fabricate a structure with four square passive hollow cuboids with $7 \times 7 \times 7$ cm^3 volume and four hollow cuboids with $9.3 \times 9.3 \times 9.3$ cm^3 volume.
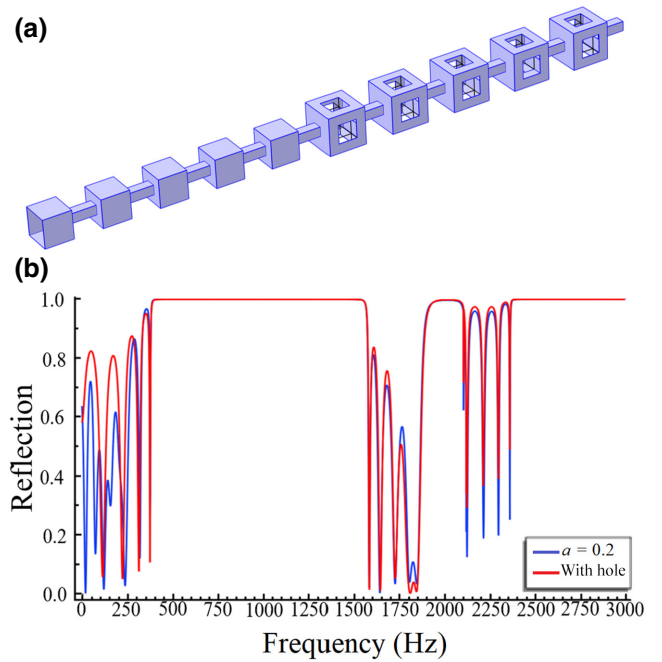

(a)

(b)

FIG. 3. (a) Schematic of realistic model where we assume large cuboids in the non-Hermitian (lossy) sublattice have the same bulk modulus as the first sublattice. We devise square holes with sides ($s = 4.6$ cm) in large cuboids to induce loss in the non-Hermitian sublattice. (b) Comparison of reflection amplitude from the realistic model (structure with embedded holes, red curve) and effective model with $a = 0.2$ (blue curve). We observe that, over most frequency ranges, the realistic model and effective model match each other.

These cuboids are connected to each other by rectangular cuboids with $7 \times 2.3 \times 2.3$ cm^3 volume. The structure is printed using a Makerbot Replicator Z18 printer with extruded PLA with a density of $\rho = 1190$ kg/m^3 and a bulk modulus of $\epsilon = 3.5 \times 10^9$ Pa. We frame square holes with sides $s = 4.6$ cm with large cuboids. To introduce loss, we cover the holes with absorbing polyester foam material, which adds loss to the system. By removing the absorbing polyester foam material and covering the holes with leads made from PLA material, we turn the structure back to the Hermitian case with a sound-hard-boundary wall without absorption. We perform our scattering experiment for both the non-Hermitian and Hermitian structures, where we measure the reflection in a homemade anechoic chamber. In the experimental setup, a 15-MHz continuous-wave synthesized-function generator is used to generate a continuous acoustic signal inside the waveguide. We capture the acoustic signals using 1/4″ omnidirectional microphones. We connect the microphones to a network analyzer via a constant-current power supply to send a low-impedance signal to the network analyzer. We observe the spectrum of our acoustic wave in the network analyzer from which we extract our data.
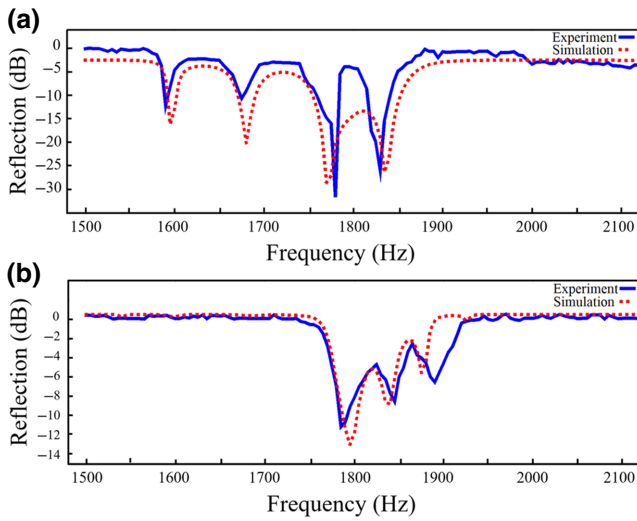
FIG. 4. Experimental realization of the tunable acoustic filter. (a) Reflection amplitude for a system with loss embedded in the system. In the experiment (blue solid curve), absorption is induced via holes that are covered by absorbing materials, while in the simulation (red dotted curve) we use the effective model with loss parameter $a = 0.2$. (b) Reflection amplitude for a system without loss, namely, no hole in the cuboids. We observe that, in the band gap, two dips appear when loss is induced in the system.

In Fig. 4, we present the experimental reflection (blue curve) and the corresponding simulation (red dotted curve) for the non-Hermitian case, with an effective model and $a = 0.2$ in panel (a) and the Hermitian case in panel (b) for $a = 0$. Here, for both, we consider 0 dB as our reference input, which is along the baseline outside of the resonance dips, where we notice very high reflection. We observe good agreement between simulation and experimental data over the frequency range 1.5–2.1 KHz. Experimental data nicely depict the filtering phenomenon that we predict. Furthermore, our experimental data agree well with the effective model over this frequency range. Notably, by increasing the number of cuboids in the Hermitian part, one can induce more resonances (as shown in our simulations), and thus, remove other frequencies from the reflected field.

V. CONCLUSION

We propose and design a tunable phononic filter based on the superposition of two sublattices, one passive and the other with variable loss. The filtering process in our proposed structure occurs in the reflected field. Apart from tunability, our filter is based on resonances, and thus, can accurately filter specific frequencies. Thus, by designing resonances in the Hermitian lattice and increasing the loss, one can remove specific frequencies on the reflected wave

at will. Our proposed tunable filter can be easily adapted to the microwave domain and to photonic structures.

[1] Y. Pennec, J. O. Vasseur, B. Djafari-Rouhani, L. Dobrzynski, and P. A. Deymier, Two-dimensional phononic crystals: Examples and applications, Surf. Sci. Rep. **65**, 229 (2010).

[2] A. Chen, Y. Wang, G. Yu, Y. Guo, and Z. Wang, Elastic wave localization in two-dimensional phononic crystals with one-dimensional quasi-periodicity and random disorder, Acta Mech. Solida Sin. **21**, 517 (2008).

[3] H. A. Arafa and A. Mehaney, Enhancement of phononic band gaps in ternary/binary structure, Phys. B. Condens. Matter **407**, 4262 (2012).

[4] Y. Xiao, J. Wen, D. Yu, and X. Wen, Flexural wave propagation in beams with periodically attached vibration absorbers: Band-gap behavior and band formation mechanisms, J. Sound Vib. **332**, 867 (2013).

[5] O. B. Matar, J. O. Vasseur, and P. A. Deymier, in *Acoustic Metamaterials and Phononic Crystals*, edited by P. Deymier, Solid-State Sciences, Vol. 173 (Springer, Berlin, Heidelberg, 2013).

[6] A. Bergamini, T. Delpero, L. D. Simoni, L. D. Lillo, M. Ruzzene, and P. Ermanni, Phononic crystal with adaptive connectivity, Adv. Mater. **26**, 1343 (2014).

[7] Z. Bian, W. Peng, and J. Song, Thermal tuning of band structures in a one-dimensional phononic crystal, J. Appl. Mech. **81**, 041008 (2013).

[8] J.-F. Robillard, O. B. Matar, J. Vasseur, P. Deymier, M. Stippinger, A.-C. Hladky-Hennion, Y. Pennec, and B. Djafari-Rouhani, Tunable magnetoelastic phononic crystals, Appl. Phys. Lett. **95**, 124104 (2009).

[9] J. Vasseur, O. B. Matar, J. Robillard, A.-C. Hladky-Hennion, and P. A. Deymier, Band structures tunability of bulk 2D phononic crystals made of magneto-elastic materials, AIP Adv. **1**, 041904 (2011).

[10] F. Allein, V. Tournat, V. Gusev, and G. Theocharis, Tunable magneto-granular phononic crystals, Appl. Phys. Lett. **108,** 161903 (2016).

[11] Osama R. Bilal, André Foehr, and Chiara Daraio, Reprogrammable phononic metasurfaces, Adv. Mater. **29,** 1700628 (2017).

[12] Z. Hou and B. M. Assouar, Tunable solid acoustic metamaterial with negative elastic modulus, Appl. Phys. Lett. **106,** 251901 (2015).

[13] P. Celli and S. Gonella, Tunable directivity in metamaterials with reconfigurable cell symmetry, Appl. Phys. Lett. **106,** 091905 (2015).

[14] Z. Wang, Q. Zhang, K. Zhang, and G. Hu, Tunable digital metamaterial for broadband vibration isolation at low frequency, Adv. Mater. **28,** 9857 (2016).

[15] P. Wang, F. Casadei, S. Shan, J. C. Weaver, and K. Bertoldi, Harnessing Buckling to Design Tunable Locally Resonant Acoustic Metamaterials, Phys. Rev. Lett. **113,** 014301 (2015).

[16] N. Boechler, G. Theocharis, and C. Daraio, Bifurcation-based acoustic switching and rectification, Nat. Mater. **10,** 665 (2011).

[17] F. Li, P. Anzel, J. Yang, P. G. Kevrekidis, and C. Daraio, Granular acoustic switches and logic elements, Nat. Commun. **5,** 5311 (2014).

[18] B. Liang, X. S. Guo, J. Tu, D. Zhang, and J. C. Cheng, An acoustic rectifier, Nat. Mat. **9,** 989 (2010).

[19] M. Caleap and B. W. Drinkwater, Acoustically trapped colloidal crystals that are reconfigurable in real time, Proc. Natl. Acad. Sci. USA **111,** 6226 (2014).

[20] X. Zhu, H. Ramezani, C. Shi, J. Zhu, and X. Zhang, PT-Symmetric Acoustics, Phys. Rev. X **4,** 031042 (2014).

[21] R. Fleury, D. Sounas, and A. Alu, An invisible acoustic sensor based on parity-time symmetry, Nat. Commun. **6,** 5905 (2015).

[22] Y. Li and B. M. Assouar, Acoustic metasurface-based perfect absorber with deep subwavelength thickness, Appl. Phys. Lett. **108,** 06302 (2016).

[23] M. Molerón, M. Serra-Garcia, and C. Daraio, Viscothermal effects in acoustic metamaterials: From total transmission to total reflection and high absorption, New J. Phys. **18,** 033003 (2016).

[24] P. M. Morse and K. U. Ingard, *Theoretical Acoustics* (Princeton University Press, Princeton, 1987).ISBN: 9780691024011

[25] E. Andreassen and J. S. Jensen, Analysis of phononic bandgap structures with dissipation, J. Vib. Acoust. **135,** 041015 (2013).

[26] R. S. Langley, On the forced response of one-dimensional periodic structures: Vibration localization by damping, J. Sound Vib. **178,** 411 (1994).

[27] J. S. Jensen, Phononic band gaps and vibrations in one- and two-dimensional mass-spring structures, J. Sound Vib. **266,** 1053 (2003).

[28] G. P. Ward, R. K. Lovelock, A. R. J. Murray, A. P. Hibbins, J. R. Sambles, and J. D. Smith, Boundary-Layer Effects on Acoustic Transmission Through Narrow Slit Cavities, Phys. Rev. Lett. **115,** 044302 (2015).

[29] L. Feng, R. El-Ganainy, and Li Ge, Non-Hermitian photonics based on parity-time symmetry, Nat. Photonics **11,** 752 (2017).

[30] J. Zhang, B. Peng, S. K. Özdemir, Y. Liu, H. Jing, X. Lü, Y. Liu, L. Yang, and F. Nori, Giant nonlinearity via breaking parity-time symmetry: A route to low-threshold phonon diodes, Phys. Rev. B **92,** 115407 (2015).

[31] Kun Ding, Z. Q. Zhang, and C. T. Chan, Coalescence of exceptional points and phase diagrams for one-dimensional PT-symmetric photonic crystals, Phys. Rev. B **92,** 235310 (2015).

[32] C. Z. Shi, M. Dubois, Y. Chen, L. Cheng, H. Ramezani, Y. Wang, and X. Zhang, Accessing the exceptional points of parity-time symmetric acoustics, Nat. Commun. **7,** 11110 (2016).

[33] J. Christensen, M. Willatzen, V. R. Velasco, and M.-H. Lu, Parity-Time Synthetic Phononic Media, Phys. Rev. Lett. **116,** 207601 (2016).

[34] H. Ramezani, M. Dubois, Y. Wang, Y. R. Shen, and X. Zhang, Directional excitation without breaking reciprocity, New J. Phys. **18,** 095001 (2016).

[35] Y. Li, C. Shen, Y. Xie, J. Li, W. Wang, S. A. Cummer, and Y. Jing, Tunable Asymmetric Transmission via Lossy Acoustic Metasurfaces, Phys. Rev. Lett. **119,** 035501 (2017).

[36] Y. Aurégan and V. Pagneux, PT-Symmetric Scattering in Flow Duct Acoustics, Phys. Rev. Lett. **118,** 174301 (2017).

[37] A. V. Poshakinskiy, A. N. Poddubny, and A. Fainstein, Multiple Quantum Wells for PT-Symmetric Phononic Crystals, Phys. Rev. Lett. **117,** 224302 (2016).

[38] A. Alevizaki, R. Sainidou, P. Rembert, B. Morvan, and N. Stefanou, Phononic crystals of poroelastic spheres, Phys. Rev. B **94,** 174306 (2016).

[39] A. Alevizaki, R. Sainidou, P. Rembert, B. Morvan, and N. Stefanou, Acoustic properties of double-porosity granular polymers, Phys. Rev. B **95,** 214306 (2017).

[40] Xu Wang, Xinsheng Fang, Dongxing Mao, Yun Jing, and Yong Li, Extremely Asymmetrical Acoustic Metasurface Mirror at the Exceptional Point, Phys. Rev. Lett. **123,** 214302 (2019).

[41] Yuzhen Yang, Han Jia, Yafeng Bi, Han Zhao, and Jun Yang, Experimental Demonstration of an Acoustic Asymmetric Diffraction Grating Based on Passive Parity-Time-Symmetric Medium, Phys. Rev. Appl. **12,** 034040 (2019).

[42] Tuo Liu, Xuefeng Zhu, Fei Chen, Shanjun Liang, and Jie Zhu, Unidirectional Wave Vector Manipulation in Two-Dimensional Space with an All Passive Acoustic Parity-Time-Symmetric Metamaterials Crystal, Phys. Rev. Lett. **120,** 124502 (2018).

[43] He Gao, Haoran Xue, Zhongming Gu, Tuo Liu, Jie Zhu, and Baile Zhang, Non-Hermitian route to higher-order topology in an acoustic crystal, Nat. Commun. **12,** 1888 (2021).

[44] Zhongming Gu, He Gao, Tuo Liu, Shanjun Liang, Shuowei An, Yong Li, and Jie Zhu, Topologically Protected Exceptional Point with Local Non-Hermitian Modulation in an Acoustic Crystal, Phys. Rev. Appl. **15,** 014025 (2021).

[45] Taehwa Lee, Tsuyoshi Nomura, Ercan M. Dede, and Hideo Iizuka, Asymmetric loss-induced perfect sound absorption in duct silencers, Appl. Phys. Lett. **116,** 214101 (2020).

[46] Taehwa Lee, Tsuyoshi Nomura, Ercan M. Dede, and Hideo Iizuka, Ultrasparse Acoustic Absorbers Enabling Fluid Flow and Visible-Light Controls, Phys. Rev. Appl. **11,** 024022 (2019).

[47] Taehwa Lee and Hideo Iizuka, Acoustic resonance coupling for directional wave control: From angle-dependent absorption to asymmetric transmission, New J. Phys. **21,** 043030 (2019).

[48] Ben Lustig, Guy Elbaz, Alan Muhafra, and Gal Shmuel, Anomalous energy transport in laminates with exceptional points, J. Mech. Phys. Solids **133,** 103719 (2019).

[49] C. Bourquard and N. Noiray, Stabilization of acoustic modes using Helmholtz and Quarter-Wave resonators tuned at exceptional points, J. Sound Vib. **445,** 288 (2019).

[50] Jianlin Yi, Mehrdad Negahban, Zheng Li, Xianyue Su, and Rongyu Xia, Conditionally extraordinary transmission in periodic parity-time symmetric phononic crystals, Int. J. Mech. Sci. **163,** 105134 (2019).

[51] H. Ramezani, D. N. Christodoulides, V. Kovanis, I. Vitebskiy, and T. Kottos, PT-Symmetric Talbot Effects, Phys. Rev. Lett. **109,** 033902 (2012).

[52] M. Dehghani, C. Yuce, T. Kottos, and H. Ramezani, Constant intensity conical diffraction in discrete one-dimensional lattices with charge-conjugation symmetry, Opt. Lett. **45,** 101 (2020).

[53] The appearance of a flat band is associated with vertical modes that are not propagating through the lattice, and thus, are irrelevant to our discussion.